International Journal of Advanced Multidisciplinary Research
ISSN: 2393-8870
www.ijarm.com
(A Peer Reviewed, Referred, Indexed and Open Access Journal)
DOI: 10.22192/ijamr Volume 13, Issue 4-2026

Research Article

DOI: http://dx.doi.org/10.22192/ijamr.2026.13.04.008

Lung cancer detection using Wasserstein self-attention Gan and Convorecurart Neural Network (CRANN)

[1*]Dr. N. Venkatesan, [2]Dr. V. Seetha Devi,
[3] Dr.S. Palani Kumar, [4]Dr. D. Balasubramanian

[1*]Assistant professor, Department of CSE, Chennai Institute of Technology, Chennai
[2]Associate professor, Department of IT, Jaya Engineering College, Thiruninravur, Chennai
[3]Professor, Department of CSBS, Veltech Multitech Dr. Rangarajan Dr. Sakunthala Engineering College, Avadi, Chennai
[4]Professor, Department of MCA, Jaya Engineering College, Thiruninravur, Chennai
[1*]Corresponding Author Email Id: *pnv121974@gmail.com*

Keywords

Region of Interest, Dual-Stacked Dilated Convolutions-enhanced U-Net framework, Teaching-Learning-Based Optimization with Cuckoo-Inspired Migration, Convo Recur Art Neural Network design.

Abstract

Live Lung cancer is widespread and frequently fatal, effective therapy depends on early and precise identification. A thorough strategy is implemented in this research project that focuses on lung cancer detection and includes many crucial phases. In this study we improve the quality and clarity of the raw images for this investigation, a complex preprocessing phase is used. The luna dataset is then methodically enriched, and the model's resilience is improved by applying picture augmentation techniques. In the third stage, the Region of Interest (ROI) is carefully retrieved from the pictures using an upgraded Dual-Stacked Dilated Convolutions-enhanced U-Net framework, ensuring accurate localization of potentially malignant regions. Then, geometry-based characteristics are used to precisely capture these ROIs' critical dimensions. An innovative hybrid optimization technique Teaching-Learning-Based Optimization with Cuckoo-Inspired Migration is added into the pipeline to produce the best classification results. Finally, an advanced Convo RecurArt Neural Network design is used to efficiently evaluate and categorize the ROIs for the crucial purpose of lung cancer classification. This architecture makes use of the strength of both convolutional and recurrent layers. This all-encompassing strategy has the potential to greatly increase lung cancer detection's accuracy and dependability, perhaps paving the way for earlier identification and more effective treatment.

1. Introduction

Lung cancer ranks among the most lethal diseases in existence. Over 7.6 million people worldwide die each year from lung cancer, according to the World Health Organization (WHO)'s most recent estimates. Furthermore, it is predicted that will be an increase in the number of persons who pass away from cancer, reaching almost 17 million by 2030 globally [1]. Only early detection of lung cancer can result in a successful treatment. MRI, isotope, X-ray, and CT are a few of the methods that may be used to identify lung cancer. The two well-known anatomic imaging modalities that are routinely used in the detection of different lung illnesses are computed tomography (CT) and X-ray chest radiography [2].CT scans are used by radiologists and medical experts to find and diagnose sickness, quickly see the morphologic extents of disease, describe its patterns and severity, and evaluate its clinical course and treatment response [3]. Spiral scans, a new feature of the volumetric CT technology, eliminate artifacts brought on by heart motion, inconsistent breathing cycles, partial volume effects, and scan speed [4].As CT technology has advanced, high-resolution CT scans have taken over as the preferred imaging technique for the identification and diagnosis of lung diseases. Although High-Resolution Computed Tomography (HRCT) provides pictures of the lung with continually improved anatomic resolution, the visual interpretation or assessment of a large number of CT picture slices remains a difficult task [5].

One of the most significant difficulties in the detection of lung cancer is the current screening methods' low accuracy, particularly in recognizing early-stage tumors and discriminating between benign and malignant lesions [6]. Despite advances in medical imaging technology like positron emission tomography (PET) scans and computed tomography (CT) scans, have enhanced our capacity to detect abnormalities in the lungs, they still have substantial drawbacks [7]. False positive results are frequent and can result in unnecessarily invasive treatments and patient concern, while false negative results might cause a delay in the detection and start of cancer therapy [8]. Ionizing radiation, which has its own set of health hazards, is also made available to people using these imaging procedures [9]. Additionally, the creation of extremely sensitive blood-based biomarkers as early detection of lung cancer is still in its infancy and lacks the specificity and accuracy required for routine clinical application [10]. In light of this, despite advancements in lung cancer detection techniques, there is still a need for more accurate, non-invasive, and affordable screening tools that are capable of identifying lung cancer in its earliest, most treatable stages while minimizing the potential risks related to false results as well as radiation exposure [11].

The suggested advanced feature selection method Teaching-Learning-Based Optimization with Cuckoo-Inspired Migration. By using these Teaching-Learning-Based Optimization with Cuckoo-Inspired Migration to optimize the [12], the classification model is guaranteed to concentrate on the elements of lung cancer images that are the most useful. They intelligently select the most significant and discriminative characteristics. ConvoRecurArt Neural Network (CRANN), a cutting-edge method in the field of deep learning, provides a substantial advancement in the solution of challenging issues requiring the merging of spatial and sequential data. Convolutional Neural Networks (CNNs) [13], Recurrent Neural Networks (RNNs) [14], and Artificial Neural Networks (ANNs) [15] all have advantages, and CRANN, a hybrid method, effortlessly combines these advantages inside a single, cogent design. By doing this, CRANN effectively combines the impressive spatial information processing powers of CNNs, the skill at managing sequential data that comes from RNNs' temporal modelling, and the generalization and learning capabilities of ANNs. With the help of this combination, a strong and adaptable instrument that can handle a variety of problems in numerous fields is created. In a wide range of applications, such as time series forecasting, natural language processing, image and video

analysis, and sequential and spatial pattern recognition, CRANN shines.

The main contribution in this works is

- The Wasserstein Self-Attention GAN enhances data augmentation by generating realistic lung cancer images, improving classification model robustness, and focusing on relevant regions, aiding precise texture analysis.
- The optimized U-Net with Dual-Stacked Dilated Convolutions effectively isolates regions of interest (ROI) from the rest of the image, facilitating accurate feature extraction for improved lung cancer image classification.
- The hybrid TLCM optimization intelligently identifies discriminative features, ensuring the classification model prioritizes informative aspects of lung cancer images, enhancing diagnostic accuracy.

2. Literature Review

In 2020 Shakeel *et al.* [16] proposed the prediction of lung cancer is made possible by a new, machine learning and image processing advancements. Non-small cell pulmonary cancer In order to detect lung cancer, CT scan dataset images are assembled. The resultant pictures may be examined for lung image quality while also decreasing noise by using the multilayer brightness-preserving approach, which carefully examines each pixel and eliminates noise. A lung CT picture with noise removed is segmented to show the affected area. Using a deep neural network that has been developed, multiple characteristics and network layers are used to segment the region extracted. Afterward, using intelligent-generalized rough hybrid spiral optimization to choose the most useful characteristics Those characteristics are categorised using an ensemble classifier and the set technique.

In 2019 Shakeel *et al.* [17] reduced the misclassification in order to enhance lung image quality and lung cancer diagnosis. The Cancer Imaging Archive (CIA) dataset provided the lung CT images, and noise was successfully eliminated by employing a weighted mean histogram equalization method. The afflicted region was subsequently segmented and the picture quality was further enhanced using the improved profuse clustering method (IPCT). The impacted region produces a number of spectral characteristics. Using deep learning application an analysis of immediately trained neural networks for lung cancer prediction is possible.

In 2019 Togacar *et al.* [18] experimented to extract features and classify data, convolutional neural networks (CNNs) were employed. While the models were being trained, the dataset was treated to image augmentation methods such cutting, zooming, horizontal rotation, and filling in order to raise the classification's success rate. Because of the AlexNet model's remarkable success, the features obtained from the final fully connected layer were separately applied as the input to the linear regression (LR), linear discriminant analysis (LDA), decision tree (DT), support vector machine (SVM), k-nearest neighbor (KNN), and SoftMax classifiers.

In 2021 Xie *et al*. [19] employed a ground-breaking to uncover early diagnostic signs for the disease, an interdisciplinary mechanism is first used to lung cancer. Machine learning methods are used with metabolomics in this process. A total of 110 lung cancer patients and 43 healthy individuals were recruited for our investigation. Targeted metabolomic research employing LCMS/MS was used to determine the levels of 61 plasma compounds. A specific arrangement of six metabolic markers allows for the differentiation between individuals with stage I lung cancer and healthy individuals. The top five metabolic biomarkers determined by the FCBF algorithm in terms of relative importance may also be employed as screening biomarkers for early lung cancer identification.

In 2021 Ibrahim *et al.* [20] focused on theidentification of COVID-19, pneumonia, and lung cancer is proposed using a multi-classification deep learning model of chest x-ray

and CT images. This combination has been used because a chest CT scan can detect abnormal features in images with more accuracy than a chest X-ray, which is less useful in the early stages of the disease. By including these two sorts of photos, the dataset size will increase, increasing classification accuracy. As far as we know, there isn't a deep learning model that can pick one of these illnesses over the other in the literature.

In 2023 Binson *et al*. [21] presented the chemical gas sensor array-based electronic-nose (e-nose) devices are capable of identifying and differentiating between exhaled breath samples from patients with various respiratory diseases as well as controls. By figuring out the volatile organic compound (VOC) concentrations and variations in the air inhaled, it is accomplished. In this case, they wanted to set lung cancer and chronic obstructive pulmonary disease (COPD) apart from controls. In-depth discussions of exhaled breath sample procedure, detection, data processing techniques, e-nose system construction, and subject selection are provided in this study. The developed device is tested on 199 people, including 93 controls, 55 COPD patients, and 51 lung cancer patients. Robustness, mobility, and cost-effectiveness are the device's key advantages.

In 2021Alzubaidi *et al.* [22] developed a collection of 1000 CT scan pictures. During the global training and testing phase, the obtained photos are pre-processed using image warping and cropping. Then, 10 distinct image feature types are used to extract global features from the images and represent each image using feature vectors. Then, detection models are built using six different machine learning techniques on the feature vectors. The local training and testing step divides each image into a set of local blocks. The successful feature types from the global phase are then extracted from each of these blocks in order to represent each of these blocks using feature vectors. These feature vectors are then used to generate detection models for each of the image blocks using the learning strategies that were effective in the global phase. According to the findings, the Haar Wavelet, Histogram of Oriented Gradients (HOG), and Gabor Filter feature types fared better than the other seven feature types.

In 2020 Hatuwal *et al*. [23]experimented a lot of time and is difficult to diagnose different forms of lung cancer. Convolutional Neural Networks can more accurately can swiftly sort different types of lung cancer into appropriate categories, which is crucial for determining the most effective course of treatment and patients' prognoses. This research project considers benign tissue, adenocarcinoma, and squamous cell carcinoma.

In 2020 Causey*et al.* [24] used data from a volumetric lung CT scan, A patient's cancer status may be ascertained using the algorithm DeepScreener. DeepScreener was built on our spatial pyramid pooling model, which came in 16th place (top 1%) out of 1972 teams when evaluated using the challenge datasets for the Data Science Bowl 2017 competition (DSB2017). They assess the algorithm in this work and find that DeepScreener consistently performs at a high accuracy level using 1449 low-dose CT scans from the National Lung Screening Trial (NLST) cohort as an independent test set. Additionally, it outperforms prior state-of-the-art methods that just employed 3D convolution and achieves an AUC of 0.892 by combining Spatial Pyramid Pooling with 3D Convolution.

In 2019 Liu*et al.* [25] proposed the possibility of deep reinforcement learning for identifying lung cancer in light of the incidence of lung tumors and the predicted 1.8 million deaths from lung cancer in 2018. The effectiveness of treatment and the length of survival can both be considerably improved by early identification and detection of lung tumours. In this study, a number of typical deep reinforcement learning models that might be used to make a lung cancer diagnosis are presented. The most common forms of lung cancer are also included, along with a description of each one's main features. There are still a lot of challenges to be solved and promising research directions to follow when utilizing deep reinforcement learning to detect lung cancer.

2.1. Problem Statement

Author & Year	Citation	Aim of the Study	Methodology Used	Problem Identification
Shakeel et al. 2020	[16]	Predict lung cancer using image processing & ML	Image processing, deep neural networks	In non-small cell lung cancer CT scans, detect lung cancer.
Shakeel et al. 2019	[17]	Enhance lung image quality and diagnosis	Weighted mean histogram equalization, deep learning	Improve lung cancer diagnosis and image quality
Togacar et al. 2019	[18]	Feature extraction and classification	Convolutional neural networks, data augmentation	Improve classification success rate for lung cancer
Xie et al. 2021	[19]	Find early diagnostic indicators using metabolomics	Metabolomic research, machine learning	Identify metabolic indicators for early lung cancer detection
Ibrahim et al. 2021	[20]	Multi-classification for COVID-19, pneumonia, and lung cancer	Deep learning, chest X-rays, CT images	Develop a deep learning model for multiple respiratory disorders
Binson et al. 2023	[21]	Recognize lung cancer and COPD using e-nose	Electronic-nose (e-nose), volatile organic compounds	Distinguish between lung cancer, COPD, and controls using breath samples
Alzubaidi et al. 2021	[22]	Develop detection models from CT scan images	Image preprocessing, feature extraction, machine learning	Using CT scan images, develop lung cancer detection models.
Hatuwal et al. 2020	[23]	Identify different forms of lung cancer	Convolutional Neural Networks (CNNs)	Classify adenocarcinoma, squamous cell carcinoma, and benign tissue with accuracy
Causey et al. 2020	[24]	Determine cancer status from lung CT scans	Spatial Pyramid Pooling, 3D Convolution	Develop DeepScreener algorithm for cancer detection from CT scans
Liu et al. 2019	[25]	Explore deep reinforcement learning for lung cancer diagnosis	Deep reinforcement learning models	Investigate the potential of deep reinforcement learning in lung cancer identification

3. Methodology

The six processes described are essential for a thorough and precise study when it comes to lung cancer diagnosis in medical imaging. In order to increase the quality and lower noise, preprocessing first entails cleaning and improving the input images. Next, picture augmentation techniques are used to broaden the dataset and support the training of robust models. Region of interest (ROI) identification, the third phase, aims to isolate the pertinent lung regions for examination. Then, significant characteristics are extracted from the ROIs using feature extraction, which is crucial for differentiating between malignant and healthy tissues. The most discriminative characteristics are then selected while dimensionality is decreased using hybrid optimization techniques. Deep learning algorithms use the chosen characteristics to build predictions and provide a precise early stage lung cancer diagnosis. The importance of each step in obtaining accurate findings is emphasized by the fact that these processes work together to provide a thorough pipeline for lung cancer detection in medical imaging.

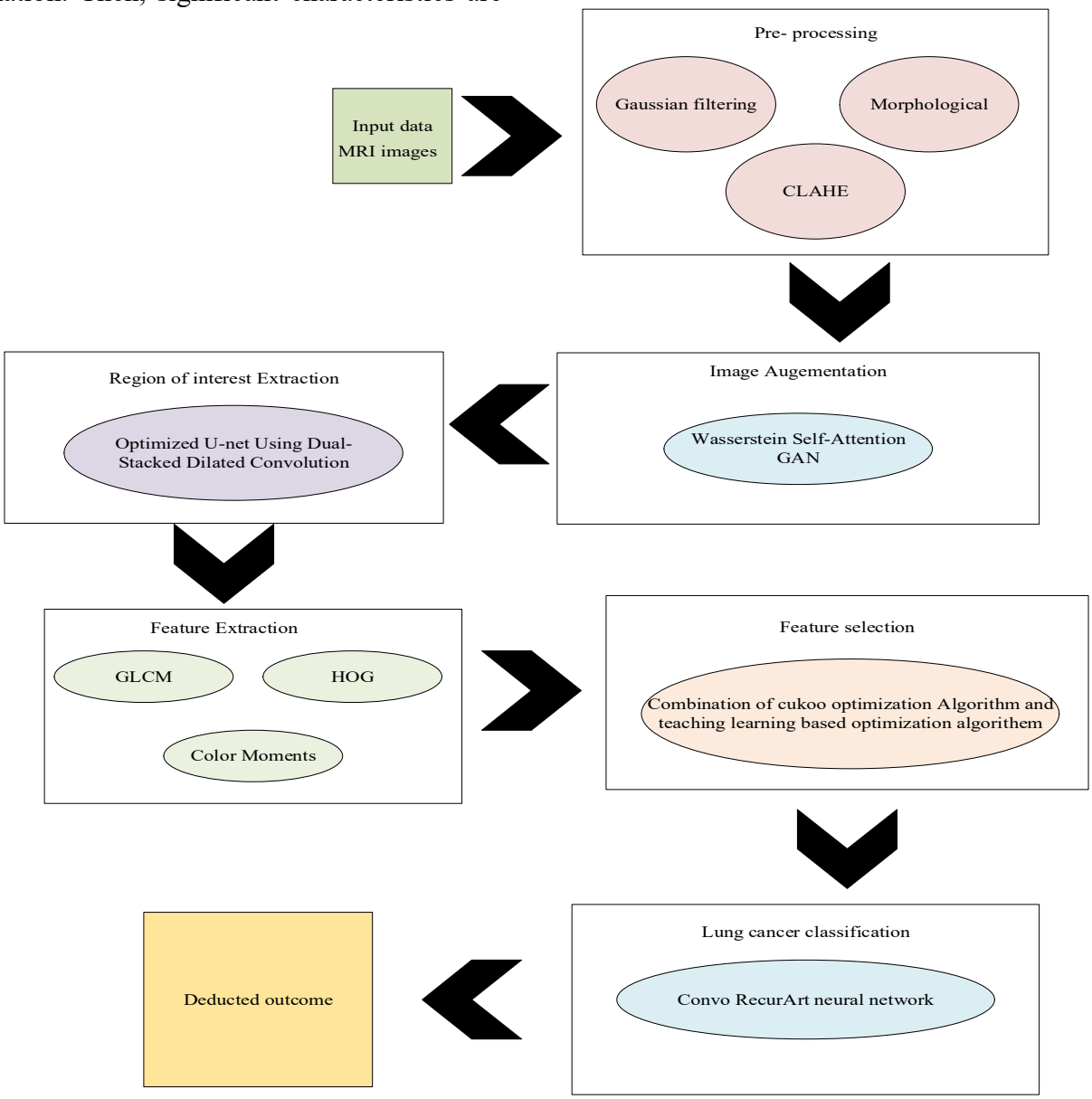

Figure 1: Architecture of the proposed model

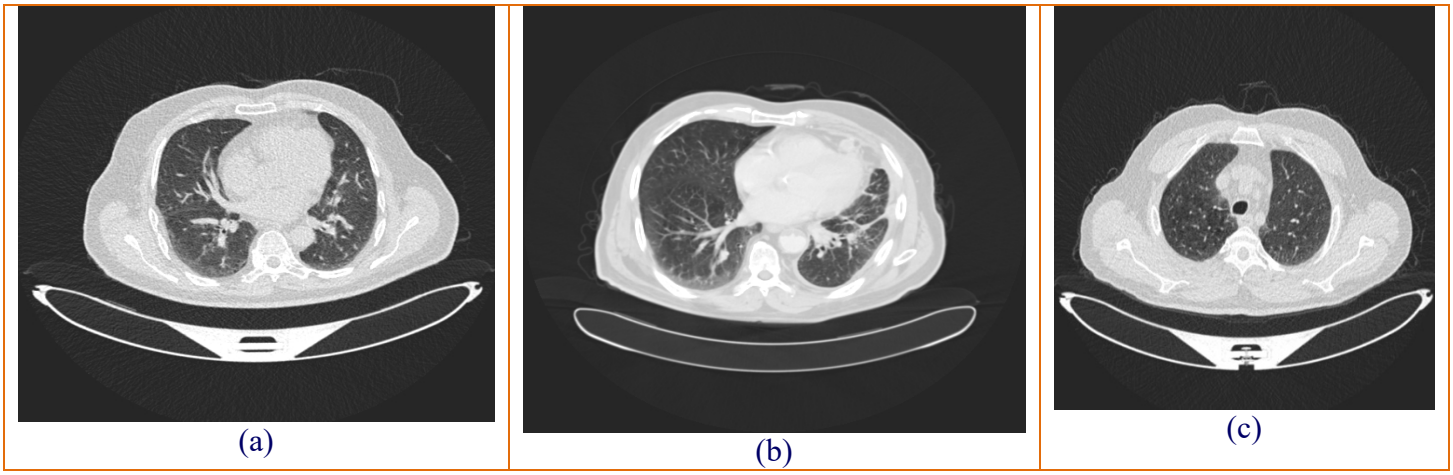

(a) (b) (c)

Figure 2: Input images

3.1. Preprocessing

Gaussian filtering (i) is used in the preprocessing stage to minimize picture noise and provide cleaner, smoother data. To improve features and remove undesired artifacts, morphological operations (ii) such erosion and dilation are utilized, which helps to improve the quality of the picture. To improve local contrast and make fine picture features easier to see, Contrast Limited Adaptive Histogram Equalization (CLAHE) (iii) is used. The combination of these techniques preserves essential picture data while raising its quality, thus increasing the precision of following analysis procedures.

3.1.1. Gaussian filtering

The input image is given a Gaussian filter. Noise may be greatly reduced by using gaussian smoothing. High frequency elements in the picture are eliminated using Gaussian. The filter is a low pass, thus. Our intensity surface is more precise after smoothing since it lowers the noise. As seen in equation (1), the mathematical formula for the Gaussian filter.

$$G(x,y) = \frac{1}{2\pi\sigma^2} e^{-\frac{(x^2+y^2)}{2\sigma^2}} \quad (1)$$

where $x$is the separation of the center from the horizontal axis, y is the vertical axis's distance, and is the gaussian distribution's σ standard deviation. The degree of smoothing is decided by it.

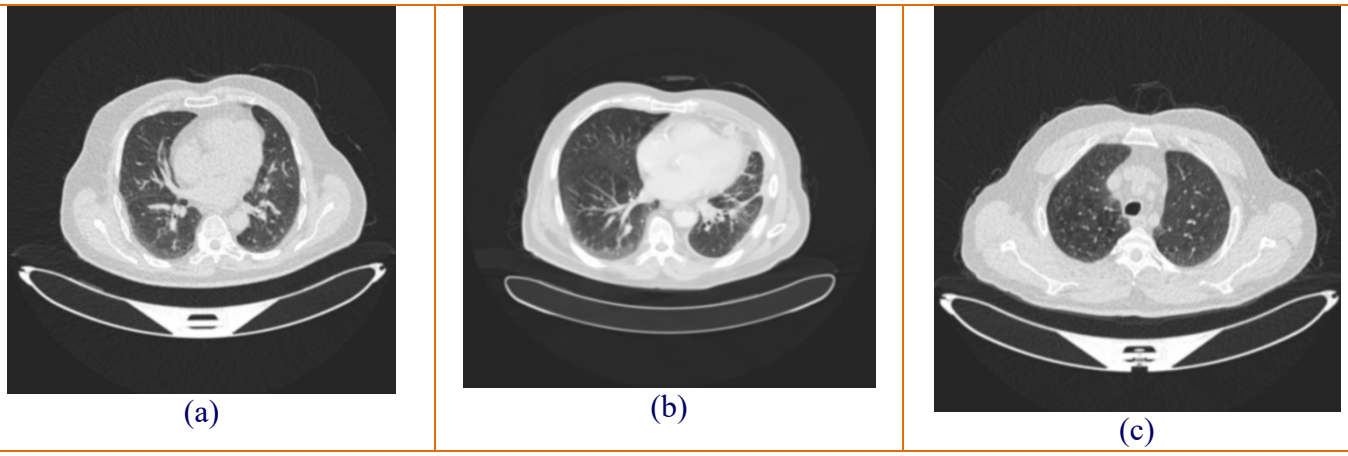

(a) (b) (c)

Figure 3: Gaussian filtering

3.1.2. Morphological

Morphological traits, especially at the microscopic or fine-scale level, relate to the structural and physical qualities of an organism or thing. In biology, it includes things like the organization, size, and shape of an organism's cells, tissues, or bodily parts; in linguistics, it refers to the way words are formed through techniques like affixation, inflection, and derivation. These characteristics are essential for categorizing, identifying, and comprehending the shape and function of numerous things across many scientific fields, providing insightful information about their underlying traits and behaviours.

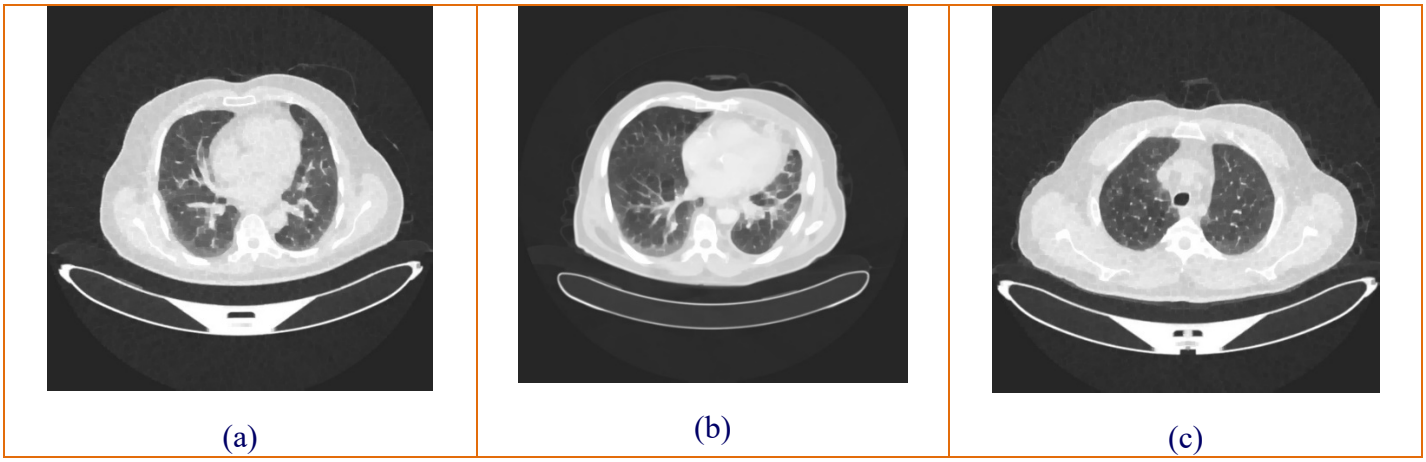

(a) (b) (c)

Figure 4: Morphological images

3.1.3. Contrast Limited Adaptive Histogram Equalization (CLAHE)

A complex picture enhancement method used to increase contrast is called CLAHE. CLAHE functions adaptively, breaking a picture into discrete sections and equalizing the histograms there instead of applying global equalization as is done with classic histogram equalization. This guarantees that noise in smooth zones won't be overly amplified due to contrast enhancement. When fine details need to be enhanced without adding artifacts, CLAHE is very helpful in computer vision and medical imaging applications. With the help of a user-defined parameter, it limits contrast amplification and prevents wildly inflated contrast levels radiology and surveillance are only a couple of the many disciplines, CLAHE is a potent tool for enhancing picture quality and exposing concealed information.

3.2. Image Augmentation

As it relates to the categorization of lung cancer images, the Wasserstein Self-Attention GAN is a unique model created for data augmentation. This technique creates artificial lung cancer pictures that closely resemble actual ones by harnessing the power of Generative Adversarial Networks (GANs). By adding these artificial pictures to the dataset to diversity it, the classification algorithm becomes more robust and is better able to recognize lung cancer patients, which eventually helps in early detection and treatment.

3.2.1. Wasserstein Self-Attention GAN

The original network model is vulnerable to gradient disappearance and mode collapse during training since GAN exists. We are going to use WGAN to fix the problem. A common occurrence during the training of a GAN is that the performance of the generator becomes difficult to enhance once the discriminator has been taught

successfully. The flaw in the GAN fundamental idea is what causes this occurrence. Following are the earliest examples of the GAN's goal function:

$$min_{\theta_g} max_{\theta_d} E_{x\sim p_{data}}[\log D_{\theta d}(x)] + E_{Z\sim P(Z)}\left[\log\left(1 - D_{\theta d}\left(G_{\theta_g}(Z)\right)\right)\right] \quad (2)$$

where, θ_d the parameters of the discriminator D, θ_g the parameters of the generator G, P_z the probability distribution of Z, and the probability distribution of are (x) actual data, (y) false data, (z) noisy data, and p_{data} is the parameters of the discriminator. It demonstrates that the ideal discriminator is when the generator is fixed.

$$D_G^*(x) = \frac{p_{data}(x)}{p_{data}(x)+p_g(x)} \quad (3)$$

in which is the data's probability distribution. However, if the discriminator is at its best, the generator's optimization goal changes to

$$C(G) = max_D\, V(G,D) \quad (4)$$

where is the objective function of the generator G and the discriminator D, and we are left with

$$C(G) = E_x{\sim}p_{data}[\log D_G^*(x)] + E_z{\sim}p_z\,[log\left(1 - D_G^*(G(Z))\right),$$
$$C(G) = E_x{\sim}p_{data}[\log D_G^*(x)] + E_x{\sim}p_g\,[log\left(1 - D_G^*(G(x))\right),$$
$$C(G) = E_x{\sim}p_{data}\left[log\frac{p_{data}(x)}{p_{data}(x)+p_g(x)}\right] + E_x{\sim}p_g\left[log\frac{p_g(x)}{p_{data}(x)+p_g(x)}\right] \quad (5)$$

The JS divergence notation may be used to express the above formula:

$$W(P_r, P_g) = inf_{y\sim\pi(p_r,p_2)} E_{(x,y)-y}[x - y_2] \quad (6)$$

where the set of all feasible joint distributions of both and the probability distribution of real samples are.

Wasserstein distance can indicate their distance even if there is no overlap between two distributions, unlike JS and KL divergence. An objective function is used to optimize Wasserstein GAN. The issue is changed to: since it is challenging to directly solve the EM distance.

$$W(P_r, P_\theta) = sup_{f_l\leq_1} E_{x\sim p\theta}[f(x)] \quad (7)$$

Once the l-Lipschitz limit has been reached, optimize the neural network settings to address:

$$max_{w \in W} E_{x \sim p_t}[f_w(x)] - E_{z \sim f(z)}[f_w(g_\theta(z))] \quad (8)$$

A new name, critic, has been given to the discriminator as well as other changes. Critic has given up on the last sigmoid layer and now outputs the score in a more broad manner rather than the likelihood like the discriminator did previously. Eq. (7) illustrates the modification to critic's objective function. Furthermore, after each update, the parameters must be clipped, or truncated, to a certain range in order to ensure the Lipschitz limit. The original GAN's vanishing gradient may be overcome by improving the generator more effectively as the critic is trained.

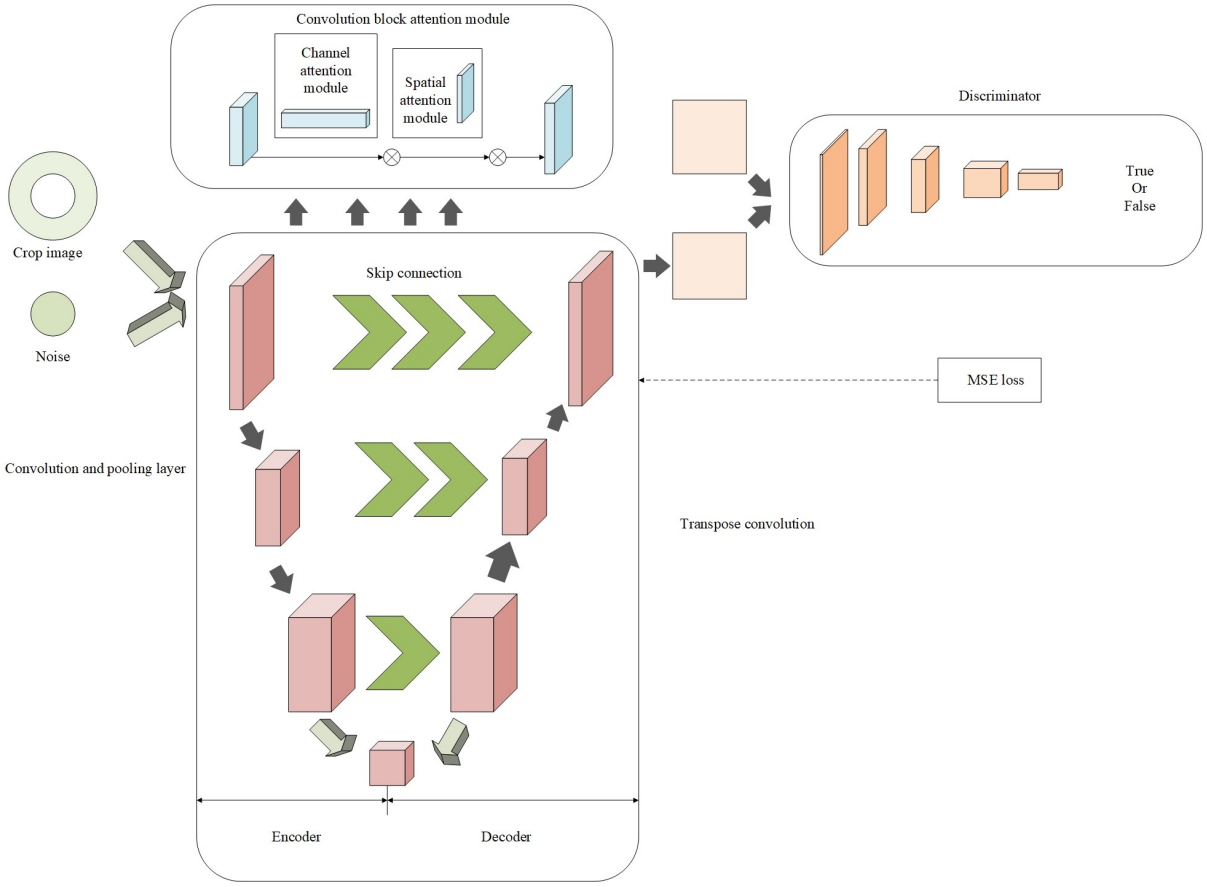

Figure 5: Wasserstein Self-Attention GAN

An improvement that promotes improved information flow within the model is the inclusion of split connections in the encoder and decoder of a Self-Attention GAN. As a result of this invention, more efficient attentional processes are made possible by the continuous processing of several input and output elements. Because of this, the model is better able to recognize complex features and distant relationships, which enhances its capacity to produce realistic and excellent images. Tasks like picture synthesis and style transfer benefit greatly from this method.

3.3. Region of Interest (ROI)

A segmentation technique is used to recognize and separate the lung tumor areas from the medical pictures. By doing this, it is made sure that the texture analysis that comes after particularly focuses on the pertinent areas. To separate the ROI region from the remainder in this research project, a dual-stacked dilated U-Net optimization technique will be used.

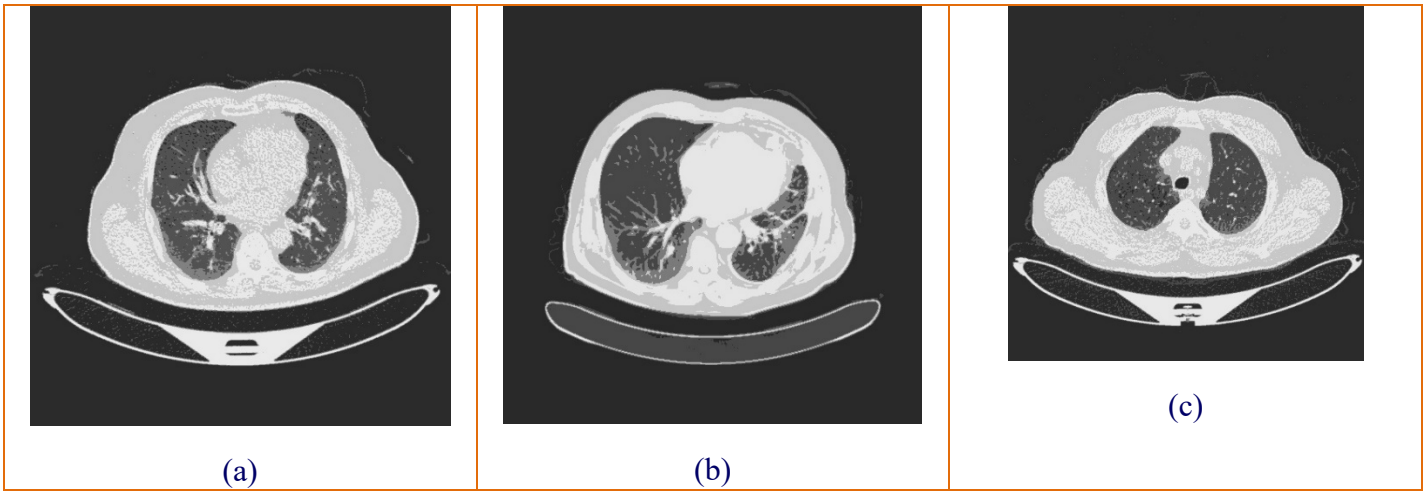

(a) (b) (c)

Figure 6: Segmented images

3.3.1. Optimized U-Net Using Dual-Stacked Dilated Convolutions

A sophisticated neural network design frequently utilized in computer vision and medical image segmentation applications is called U-Net with dual-slacked dilated convolution. By combining dual-slacked dilated convolutions and employing weight functions Teaching-Learning-Based Optimization with Cuckoo-Inspired Migration, this design expands on the conventional U-Net model. Semantic segmentation tasks are recognized for being successfully completed using the U-Net architecture. The encoder captures features from the input picture, and the decoder creates a segmented output in this encoder-decoder structure. Dilated convolutions with two different dilation rates are added by dual-slacked dilated convolutions to improve this design. As a result, the model is better able to handle objects of varied sizes inside an image since it can collect both local and global context.

The model's training and performance must be improved by optimizing the Teaching-Learning-Based Optimization with Cuckoo-Inspired Migration procedure with weight functions. In the segmented output, distinct classes or regions of interest are given varying degrees of priority using weight functions. Through better segmentation accuracy, the model is better able to concentrate on difficult areas. To achieve a compromise between recall and precision, the hybrid optimization strategy frequently mixes weight functions and many loss functions, such as dice loss or cross-entropy loss. In addition to ensuring accurate item identification, it also guarantees that the model generalizes effectively to other contexts.

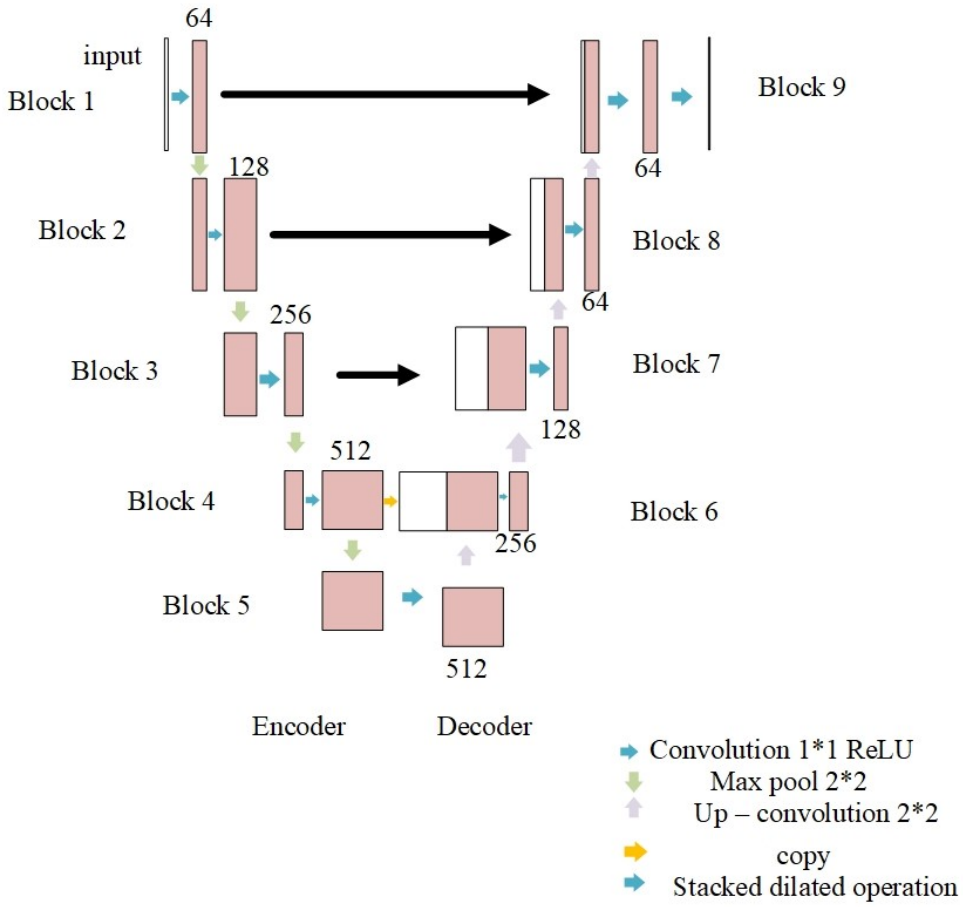

Figure 7: Optimized U-Net Using Dual-Stacked Dilated Convolutions

3.4. Feature extraction

In this feature extraction process hear we used some models such as gray-level co-occurrence matrices (GLCM), Histogram of Oriented Gradients (HOG); Color-based Features- Colour Moments.

3.4.1. Gray-level co-occurrence matrices

Gray level co-occurrence matrix, which has a huge dimension, is often not utilized as a feature to directly discriminate textures, but other statistics built on it, including entropy, contrast, correlation, etc., are used as features for texture classification. Here is a quick overview of several GLCM characteristics that are typical:

Contrast

Contrast evaluates the regional differences in the pixel's degree of gray in the co-occurrence matrix. Utilizing the following equation, the intensity of the grey picture pixels is determined:

$$\sum_{i,j=0}^{N-1}(i-j)^2 P_d(i,j) \quad (9)$$

Hence, in a GLCM matrix, $P_d(i,j)$ is the likelihood of finding adjacently occuring pixel pairs.

Homogeneity

The distribution of pixels known as homogeneity measures and calculates the degree to which the diagonal components of a GLCM matrix are near to one another. Very few gray pixels are present in homogeneous pictures, which results in high measurements for the probabilities of i, j and high sum of square values. For a diagonal, the homogeneity value is 1. Following is the equation used to compute it:

$$\sum_{i,j=0}^{N-1} \frac{1}{1+(1-j)^2} P_d(i,j) \quad (10)$$

3.4.2. Histogram of Oriented Gradients

The HOG descriptor is used for pedestrian identification, human detection, and object detection. The magnitude and direction of HOG are calculated. It is based on the accumulation of gradient axes across the pixel of a very small spatial area called a "cell" and in the subsequent construction of a 1D histogram whose concatenation gives the characteristics vector to be taken into consideration in the future. Let L represent a function of intensity (grayscale) that describes the image under study.cells of size NN pixels are used to segment the image, and the orientation of the gradient in each pixel (x, y) is calculated using the following equation:

$$\theta_{x,y} = tan^{-1} \frac{L(x,y+1) - L(x,y-1)}{L(x+1,y) - L(x-1,y)} \quad (11)$$

Successively, the orientations $\theta_i^j = 1 \ldots \ldots N$ being all belong to the same cell, j, when quantized and aggregated into an M-bins histogram. As the end result of this algorithmic phase and the features vector to be taken into consideration for further processing, all the obtained histograms are finally ranked and concatenated into an individual HOG histogram. The pre-processed face picture is separated into NN pixel-sized cells in this HOG architecture. The orientation of every pixel is computed and combined into an M-bins histogram of orientations. Following that, the final features are created by concatenating all of the cell histograms.

The orientation bines and cell size are often the two key factors used to determine the HOG descriptor's properties. Cell size serves as a representation of the patch dimension used in the generation of a single histogram. It's crucial to pick the parameters properly to improve the performance of the classification algorithm. Variations in cell size have an impact on the features retrieved using HOG. The contribution is less significant when using larger cells since the spatial information for a particular spot in a facial picture is crowded into the unit cell histogram. Smaller cells, however, may be used for high resolution examination, leading to more thorough results.

3.4.3. Color-based Features- Color Moments

Scaling and rotation are inert to colour moments. Since the majority of the information about the colour distribution is found in the low-order moments, image retrieval programs typically only employ the first three colour moments as features. Color moments are useful under changing illumination circumstances because they encode both shape and colour information, but they struggle to deal with occlusion. For any color model, color moments may be calculated. In the case of CMYK and RGB color models, respectively, 12 and 9 color moments are computed per channel, for a total of three colour moments. The same process used to calculate probability distribution moments may also be used to calculate color moments.

Mean

The first colour moment can be interpreted by using the formula below, which can then be used to calculate the average colour in the image.

$$F_k = \sum_{s=1}^{M} \frac{1}{M} G_{ks} \quad (12)$$

Standard deviation

The standard deviation, which is the second colour moment, is calculated by calculating the square root of the colour distribution's variance.

$$\sigma_k = \sqrt{\left(\frac{1}{M} \sum_{s=1}^{M} (G_{ks} - F_k)^3\right)} \quad (13)$$

Skewness

Skewness is the third colour moment. It provides data on the degree of asymmetry in the colour

distribution and, as a result, information on the distribution's shape. With the following formula, skewness can be calculated:

$$S_k = \sqrt[s]{\left(\frac{1}{M}\sum_{s=1}^{M}(G_{ks} - F_k)^3\right)} \quad (14)$$

Kurtosis

The fourth colour moment, kurtosis, offers details on the nature of the color distribution, just like skewness does. Kurtosis is a measurement of the extremeness of the tails in relation to the normal distribution.

3.5. Teaching-Learning-Based Optimization with Cuckoo-InspiredMigration (TLCM)

Within TLBO, apply the concept of COA is applied

A population-based technique called the TLBO algorithm is used to tackle the issue at hand by simulating teaching and learning activities in a classroom. The instructor phase and learner phase are the two stages that make up TLBO. The pupil who received the highest grade during the teacher phase. It is chosen from among the population to be the instructor. Training the students is the teacher's responsibility, and the class's average grade being raised. During the learner phase, each learner chooses a different learner at random to engage with.

Initialize the learner population as follows: learner

$X = \{X_{11}, X_{12}, \ldots\ldots, X_{i\,k}, \ldots X_{NM}\}$where $X_{i\,k}$ is the number of facings allotted to product i on shelf k. Equation (15) was used to produce the number of facings:

$$X_{ik} = X_{ik}^{min} + rand(0,1)\left(X_{ik}^{max} - X_{ik}^{min}\right) \quad (15)$$

It should be noted that all learners whose X_{ik} must adhere to the restrictions have X_{ik}^{min} and X_{ik}^{max}, which stand for the upper and lower boundaries of X_{ik}, respectively.

Fitness matrix

Fit= Max(A)
A- Accuarcy

based on the computed fitness first 10% of the soluation--considered as teachers, and the rest considered as students.

Evaluate the grade of learners

The learner's grade or objective value may be obtained by entering the learner's X_{ik}(choice variables) value into the objective function. The learner with the highest grade can then be chosen as the instructor and set toX_{best}.

Let M represent the class mean in the teacher's phase. The instructor makes an effort to raise M to his or her level (X_{best}) throughout this phase. Equation (16) may be used to represent the distinction between the instructor and the students:

$$Difference_{Mean} = r\left(X_{best} - T_f\, M\right) \quad (16)$$

where T_f is the teaching factor, which determines the change in mean grade, and r is a random value between $[0, 1]$. With equal chance, a random process determines the value of T_f, which has two possible values: $1\ and\ 2$.

$$T_f = \text{round}\,[1 + \text{rand}(0, 1) * (2 - 1)] \quad (17)$$

The DifferenceMean, in the context of calculating the difference in mean grades, represents the numerical value that quantifies the disparity between two sets of mean grades. To compute this difference, you would typically subtract the mean grade of one group or dataset from the mean grade of another.

$$\text{Difference Mean} = T_f * (X_{best} - \text{M}) \quad (18)$$

To update each learner's solution (X$newik$), calculate the difference in mean grades between their current solution and the desired outcome, then multiply it by the Migration Coefficient (F) to determine the adjustment magnitude. Apply this adjustment to each learner's solution iteratively to converge towards the target outcome. Repeat this process until the desired improvement is achieved in a few iterations. This dynamic updating strategy optimizes performance and adapts to changing conditions effectively.

$$Xnewik = X_{ik} + F * Difference_{Mean} \quad (19)$$

Self-Learning Model

Self-learning is a process where individuals continually refine their solutions using their current knowledge and experiences. It embodies the belief that personal growth and improvement stem from one's own journey and reflections. This approach acknowledges that individuals have the capacity to adapt, learn, and innovate through their unique life experiences. It promotes self-reliance and empowers individuals to evolve independently. Ultimately, self-learning is a dynamic, ongoing process of self-improvement driven by personal insight and development.

Mathematical Expression:

For Student i:

$$Xnew_i = Xold_i \quad (20)$$

$Xnew_i$ represents the updated position of a specific student, while $Xold_i$represents their current position. The transition from $Xold_i$ to $Xnew_i$ typically involves some form of computation or algorithm that might depend on factors like optimization objectives, constraints, or peer influence. This process is central to iterative algorithms such as optimization methods, machine learning, or simulations, where students, or entities, continually adjust their positions to improve their performance or adapt to changing conditions. The effectiveness of these updates plays a crucial role in achieving desired outcomes within the given problem or system.

Learning from Others (Peers) Model:

This model employs social learning, where individuals in a population learn from their peers. Students update their solutions by observing and incorporating the positions of randomly selected fellow students. This process mimics the way knowledge spreads through social interactions, allowing for collective problem-solving and adaptation over time. It can be applied in various contexts, from optimization problems to educational simulations, fostering collaborative learning and innovation.

Mathematical Expression:

For Student i:

$$Xnew_i = Xnew_i + \text{rand}(0, 1) * (X_{peer} - Xold_i) \quad (22)$$

Where:

Each student's updated position, denoted as $Xnew_i$, is determined based on their current position, $Xold_i$, and the position of a randomly selected peer, X_{peer}. This process introduces an element of randomness and social interaction into individual learning. It allows students to incorporate insights or strategies from their peers into their own positions, promoting diversity and exploration within the population. Such interactions can lead to collective adaptation and the emergence of novel solutions in various problem-solving scenarios.

Learning from Teachers Model:

During the teaching phase, pupils get knowledge from the perspectives of one or more members of the population who are viewed as being more successful or knowledgeable. Every student revises their response in light of the professors' perspectives.

Mathematical Expression:

For Student *i*:

$$Xnew_i = Xold_i + rand(0, 1) * (X_{teacher} - Xold_i) \quad (23)$$

Where:

In this model, the updated position of student i, represented as $Xnew_i$, is determined based on their current position, $Xold_i$, and the guidance provided by a teacher, denoted as $X_{teacher}$. This teacher may represent an expert or a source of knowledge in the context of learning or optimization. The students adapt their positions by incorporating information or insights from the teacher, which can be a crucial mechanism for transferring knowledge and fostering skill development. This approach can be valuable in educational settings, optimization algorithms, or any scenario where mentorship or external guidance is essential for improving individual performance.

Termination: Verify that the halting condition has been satisfied (the maximum number of generations have been produced). The algorithm concludes and outputs the current solution, which is the best possible solution for this generation, if the criteria is satisfied. If not, it evaluates each student's grade in preparation for the following teacher phase.

3.6. Convo RecurArt Neural Network

A key development in deep learning models is the ConvoRecurArt Neural Network (CRANN), which offers a thorough strategy for resolving complex problems that inherently involve both spatial and sequential data. This innovative hybrid architecture skillfully combines Convolutional Neural Networks (CNNs), Recurrent Neural Networks (RNNs), and Artificial Neural Networks (ANNs), ushering in a new age of deep learning capabilities. When used for a variety of tasks involving the integration of spatial and temporal information, such as computer vision tasks and natural language processing, CRANN proves to be a versatile and formidable tool.CRANN is a powerful tool for jobs requiring images, video frames, or any other data with spatial structures since it fundamentally uses CNNs to extract complex spatial properties from data. CNNs perform better in tasks like picture classification, object identification, and facial recognition because they are excellent at spotting patterns and hierarchical representations in these domains. However, a lot of real-world issues go beyond simple snapshots or static pictures and need for a comprehension of temporal connections. The RNN-synergy is essential in this situation. RNNs are the preferred method for applications like speech recognition, time-series forecasting, and natural language comprehension because of their prowess with sequential data. As a result of the seamless integration of RNNs into the CRANN architecture, the model has a built-in ability to recognize the temporal context of the data, which enables it to perform exceptionally well in tasks involving dynamic and developing information.

The merging of CNNs and RNNs is only the beginning of CRANN. ANN components are also included, giving the model an additional level of generalization and flexibility. End-to-end learning and optimization are made possible by ANNs, which act as the link between the sequential and spatial processing capacities of CNNs and RNNs. In addition to improving classification performance, this all-encompassing strategy enables CRANN to take on challenging tasks like autonomous driving, video analysis, and medical picture diagnostics, where the interaction between spatial and sequential data is crucial. The development process is streamlined by combining all three neural network paradigms into a single model, which eliminates the need for intricate assembly methods and results in a more effective and understandable solution. The CRANN model's intrinsic capabilities are used by fine-tuning its weights using cutting-edge approaches, which improves classification performance across a variety of domains. This dynamic method makes CRANN a useful tool for machine learning practitioners and academics since it allows it to adjust to the peculiarities of certain tasks and datasets. Conclusively, the ConvoRecurArt Neural Network (CRANN) is a ground-breaking combination of CNNs, RNNs, and ANNs that provides a flexible and effective response to

challenging data-driven problems. As a result, it limits of what is possible in the field of deep learning thanks to its capacity to seamlessly combine spatial and sequential data.

excels in a variety of applications and pushes the

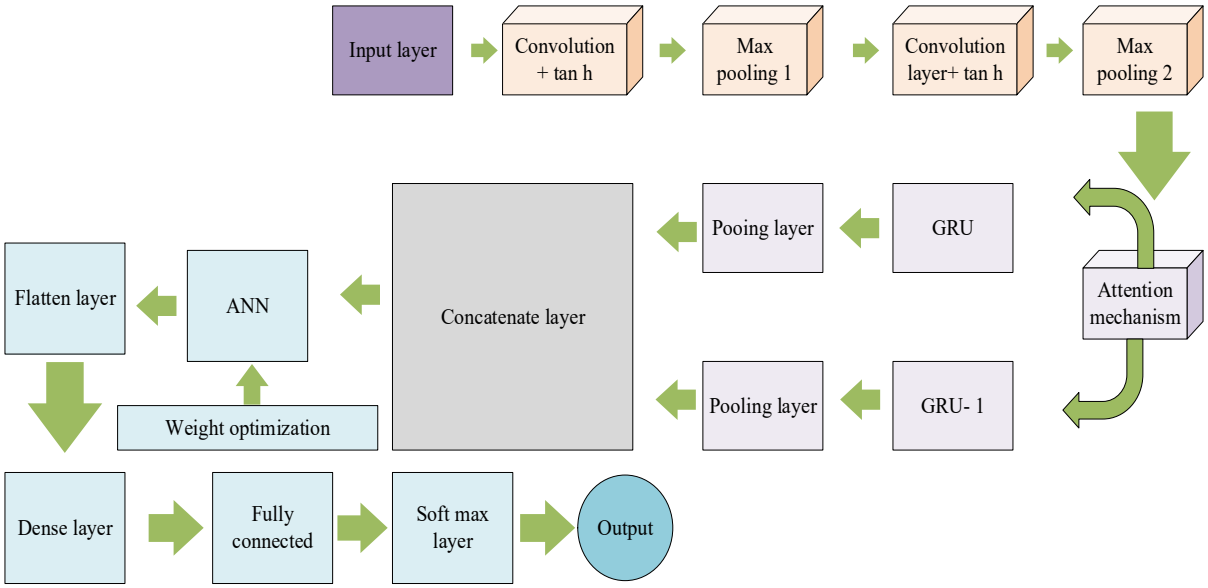

Figure 8: Convo RecurArt Neural Network

4. Result and Discussion

4.1. Dataset

The resolution of the scanner determines how many slices, or z, are used in a CT scan, gives rise to pictures with a size of (z, 512, 512). The limitation of the computer capacity prevents the direct feeding of such huge pictures into Convolution Network structures. The locations where cancer is most prone to occur must thus be determined. We will be able to concentrate our search by segmenting the lungs first, and then removing the low intensity regions. The reading of the dataset and its visualization will be the initial steps in this session. After segmenting the various lung components, we'll employ image processing methods to search for the region of interest (possible cancer spots) in the CT images. Because there is no uniformity in the lung region, the pulmonary structures have similar densities, despite the fact that there are many scanners and scanning techniques, segmenting the lung structures is a highly challenging task. The segmented lungs may also be utilized to identify regions of interest and potential lung nodule candidates, which may aid in better classifying CT scans. Finding the nodule areas in the lung is a very difficult process since some nodules are connected to blood vessels or are situated at the region's border. The lung nodule candidates may then be utilized for classification by taking out the 3D voxels surrounding them and putting the data through a 3D CNN that can be trained using the LUNA16 dataset.

https://www.kaggle.com/code/arnavkj95/candidate-generation-and-luna16-preprocessing (26)

Precision, accuracy, specificity, sensitivity, F-Measure, MCC, NPV, FPR, and FNR are some of the confusion matrix metrics used for assessing performance. In this section, the equation used for computing metrics is presented.

i) Accuracy

By comparing the percentage of cases that were correctly predicted to all other occurrences, reliability is assessed.

$$Accuracy = \frac{TP + TN}{TP + FP + FN + TN}$$

ii) Precision

As a key metric for measuring how well the positive chemicals are predicted, precision calculates the ratio of positively anticipated positive occurrences to all test results.

$$Precision = \frac{TP}{TP + FP}$$

iii) Sensitivity

By subtracting the total positives from the percentage of accurate positive forecasts, the sensitivity value can be obtained.

$$Sensitivity = \frac{TP}{TP + FN}$$

iv) Specificity

The degree of specificity is the proportion of issues that might have been avoided that were really caused all undesirable outcomes.

$$Specificit\ y\ = \frac{TN}{TN + FP}$$

v) F- Measure

A single type of data item must be present in each class, which is why the F-Measure integer was developed to correctly identify every information bit.

$$F\_Score = \frac{Presision.\ Recall}{Presision +\ Recall}$$

vi) Matthew's correlation coefficient (MCC)

The correlation measurement of the binary two-by-two variable of the MCC is depicted in the graph below.

$$MCC = \frac{(TP \times TN - FP \times FN)}{\sqrt{(TP + FN)(TN + FP)(TN + FN)(TP + FP)}}$$

vii) Negative Prediction Value (NPV)

NPV is used to evaluate a diagnostic test's effectiveness or the efficacy of a comparable quantitative indicator.

$$NPV = \frac{TN}{TN + FN}$$

viii) False Positive Ratio (FPR)

False positives are examples of negative events that were mistakenly classified as positive; the frequency of false positives is calculated by dividing the total number of negative events by the percentage of false positives.

$$FPR = \frac{FP}{FP + TN}$$

xi) False Negative Ratio (FNR)

The possibility that a true positive will not be detected by the test is called the "miss rate," often referred to as the "false-negative rate."

$$FNR = \frac{FN}{FN + TP}$$

Table 2: Metrices analysed

	ANN	CNN	RNN	PROPOSED
Accuracy	0.9074	0.9490	0.9259	0.96759
Precision	0.8611	0.9236	0.8888	0.95138
Sensitivity	0.8611	0.9236	0.8888	0.95138
Specificity	0.9305	0.9618	0.9444	0.97569
F-Measure	0.8611	0.9236	0.8888	0.95138
MCC	0.7916	0.8854	0.8333	0.92708
NPV	0.9305	0.9618	0.9444	0.97569
FPR	0.0694	0.0381	0.0555	0.02430
FNR	0.138	0.0763	0.1111	0.04861

Accuracy

The accuracy results for several neural network topologies and a Proposed Model, are shown in Table 2. The ANN's accuracy of 0.9074 demonstrated its usefulness for the task at hand, although there was potential for improvement. With an accuracy of 0.9490, the CNN surpassed ANN, showcasing its capacity to identify spatial elements in data, which are frequently essential for jobs like picture identification. With an accuracy of 0.9259, RNN also performed well, demonstrating its applicability for sequential data processing. With an astounding accuracy of 0.96759, the Proposed model outperformed all others, indicating that it uses novel methods or architectural changes to become the most effective option for the task at hand. The analyed graph are mentioned below in Figure 9.

Precision

Precision is a measure of how effectively these models properly categorize relevant cases and the accuracy of their positive predictions. The outcomes show that the suggested model surpassed the other designs in terms of producing precise positive predictions, earning the greatest accuracy score of 0.95138. Additionally, CNN showed excellent accuracy at 0.9236, demonstrating its efficiency in properly categorizing pertinent cases. ANN and RNN behind the planned and CNN by a small margin although still attaining good precision ratings of 0.8611 and 0.8888, respectively.The analyed graph are mentioned below in Fig 10.

Sensitivity

In table 2 the suggested model performs better than the other neural network topologies, with a higher sensitivity score of 0.95138. This shows that the suggested model performs better at accurately identifying positive situations, giving it an attractive option for jobs where precise identification of positives is essential. The CNN also performs well, as evidenced by its sensitivity of 0.9236, which points to its applicability for applications requiring spatial or picture data. The ANN and RNN, on the other hand, have lower sensitivity ratings, emphasizing their possible limits in this particular situation. The analyed graph are mentioned below in Figure 11.

Specificity

In Table 2, the classification problems, the metric of specificity is used to assess how well a model can distinguish between the real negatives and all other instances of actual negative behavior. The suggested model performs better in this instance in accurately classifying negative situations, as evidenced by its maximum specificity value of 0.97569. This shows that the suggested approach is successful in differentiating non-targeted cases, which is important in many applications, such as medical diagnosis or fraud detection. Additionally, CNN performs admirably with a specificity of 0.9618, whereas ANN and RNN have somewhat lower specificity scores of 0.9305 and 0.9444, respectively. The analyed graph are mentioned below in Figure 12.

F-Measure

Table 2 shows that the suggested model surpasses the others in terms of F-Measure when comparing several neural network designs (ANN, CNN, RNN), as well as the proposed model itself. Higher values of the F-Measure indicate overall superior performance since it is frequently used to measure how accuracy and recall balance in classification tasks. The suggested model successfully classified and balanced both true positives and false positives/negatives, as evidenced by its remarkable F-Measure of 0.95138. Despite having the second-highest F-Measure at 0.9236, the CNN's performance is inferior to that of the suggested model. With F-Measures of 0.8888 and 0.8611, the RNN and ANN trail even farther. The analyed graph are mentioned below in Fig 13.

MCC

The Matthew's Correlation Coefficient (MCC) values for several neural network designs, such as ANN, CNN, RNN, and a Proposed model, are

included in the table 2. MCC is a statistic that's used to assess how well categorization models work; greater values signify a model's ability to anticipate outcomes. With a remarkable MCC of 0.92708, the Proposed model shines out in this comparison and indicates that, in contrast to the other designs, it is superior at classification tasks. While ANN and RNN have significantly lower MCC values of 0.7916 and 0.8333, respectively, CNN also performs well, with an MCC of 0.8854. The analyed graph are mentioned below in Figure 14.

Negative Prediction Value

In the Table 2, several neural network models, including suggested models and ANN, CNN, and RNN, are compared. The following outcomes are obtained from measuring each model's performance using the metric of Negative Prediction Value(NPV): The suggested model outscored them all with an NPV of 0.97569, whereas ANN, CNN, and RNN all obtained NPVs of 0.9305, 0.9618, and 0.9444, respectively. These NPV values show how well the models can forecast the future or make judgments today; a larger NPV indicates better performance. By having a much larger NPV than the other neural network topologies taken into consideration, the suggested model has the potential to be a better option for the task at hand.The analyed graph are mentioned below in Figure 15.

FPR

The suggested model beats the others in terms of False Positive Rate (FPR) in a comparative examination of machine learning models. The FPR for ANN, CNN, and RNN are 0.0694, 0.0381, and 0.0555, respectively, whereas the FPR for the suggested model was an amazingly lower 0.0243. This means that, when compared to the conventional ANN, CNN, and RNN architectures, the suggested model shows greater accuracy in properly recognizing negative situations with a markedly lower number of false alarms. The analyed graph are mentioned below in Figure 16.

FNR

The False Negative Rate (FNR), in particular, is presented in Table 2. The proportion of events mistakenly labeled as negative when they were positive is shown by the FNR values. When comparing the topologies, the Proposed model stands out as having the lowest FNR of 0.04861, demonstrating its improved capacity to detect positive situations with accuracy while minimizing false negatives. In contrast, ANN has the greatest FNR of 0.138, indicating a worse ability to recognize positive situations. With FNR values of 0.0763 and 0.11, respectively, CNN and RNN fall between these two. The analyed graph are mentioned below in Figure 17.

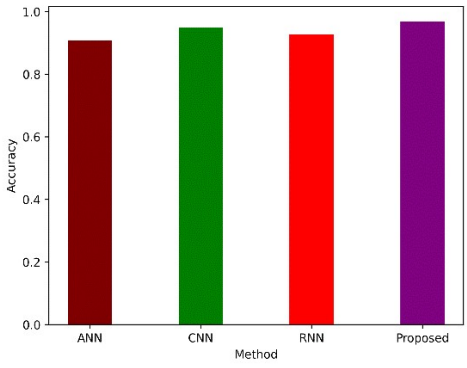

Figure 9: Accuracy

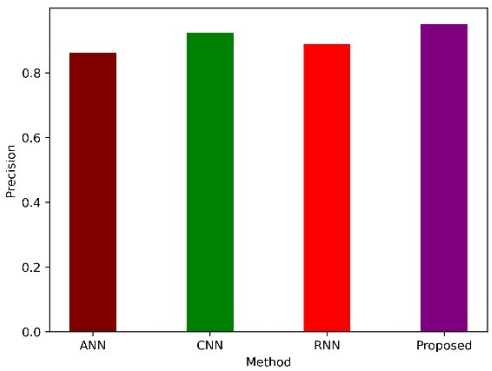

Figure 10: Precession

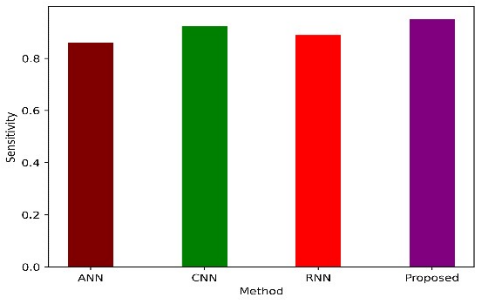

Figure 11: Sensitivity

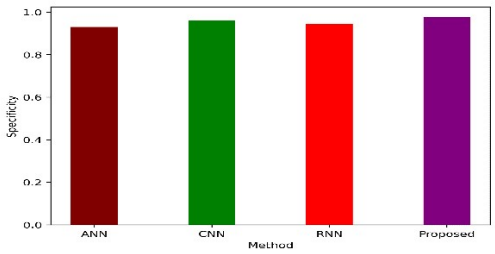

Figure 12: Specificity

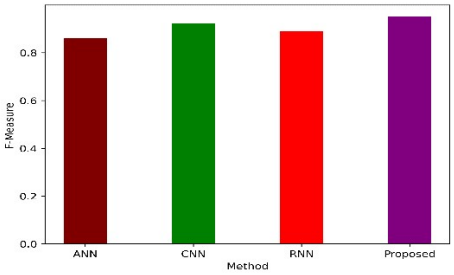

Figure 13:F- Measure

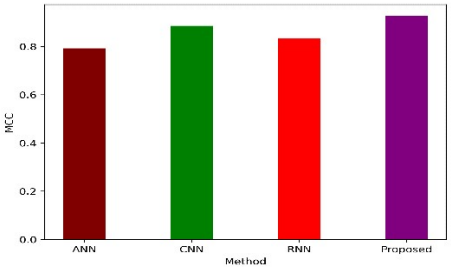

Figure 14: Matthew's Correlation Coefficient

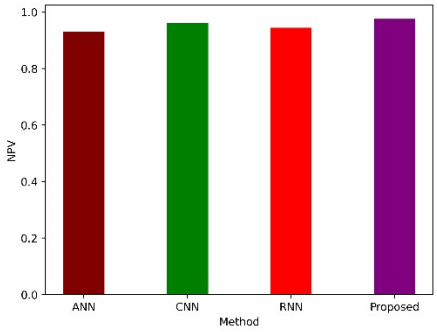

Figure 15: Negative Prediction Value

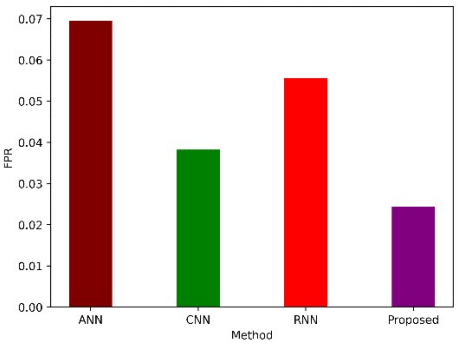

Figure 16: False Positive Rate

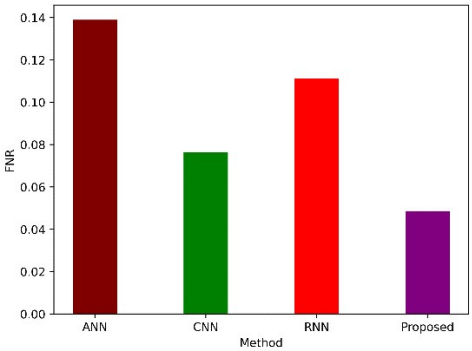

Figure 17: False Negative Rate

4.2. Comparision Analysis

- Plot 1 has analysed the comparision betwee Accuracy and Precession are shown in Figure 18.
- Plot 2 has analysed the comparision between Sensitivity and specificity are shown in Figure 19.
- Plot 3 has anlaysed the comparision between F- Measure, MCC, NPV are shown in Figure 20.
- Plot 4 has analysed the comparision between FPV, FNR are shown in Figure 21.

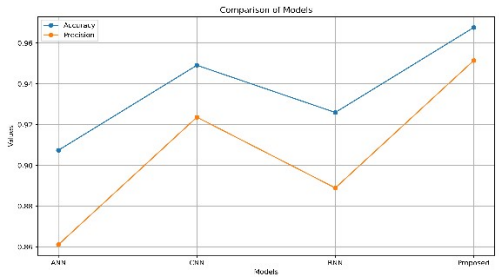

Figure 18: Accuracy and Precession

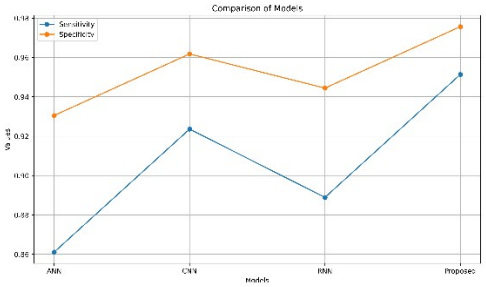

Figure 19: Sensitivity and specificity

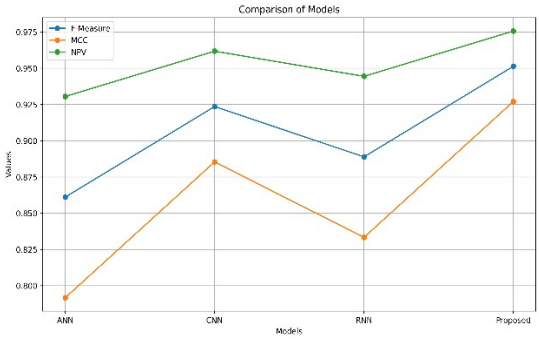

Figure 20:F- Measure, MCC, NPV

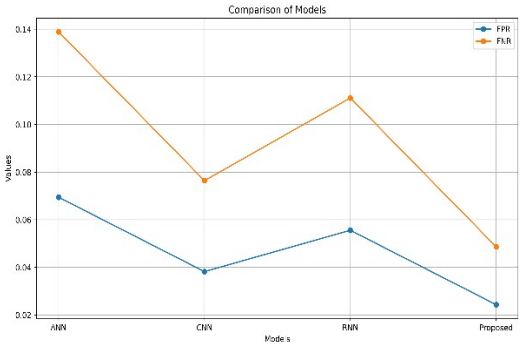

Figure 21:FPV, FNR

5. Conclusion

In conclusion, this comprehensive research project represents a multifaceted approach to enhancing lung cancer detection and diagnosis. By addressing various critical stages, from image preprocessing to region of interest localization, dimension characterization, and optimization techniques, this study demonstrates a dedication to improving both the quality and precision of early lung cancer identification. The innovative hybrid optimization technique, along with the advanced Convo RecurArt Neural Network design, showcases the commitment to pushing the boundaries of current technology for the benefit of patients. Ultimately, this holistic strategy holds great promise in significantly increasing the accuracy and reliability of lung cancer detection, potentially leading to earlier diagnoses and more effective treatment options, thereby making a substantial impact on patient outcomes and healthcare advancement.

Declarations

Data availability statement

All the data is collected from the simulation reports of the software and tools used by the authors. Authors are working on implementing the same using real world data with appropriate permissions.

Funding

No fund received for this project

Conflicts of interest

The authors declare that they have no conflict of interest.

Ethical approval and human participation

No ethics approval is required.

References

[1]. Asuntha, A. and Srinivasan, A., 2020. Deep learning for lung Cancer detection and classification. *Multimedia Tools and Applications*, *79*, pp.7731-7762.

[2]. Nooreldeen, R. and Bach, H., 2021. Current and future development in lung cancer diagnosis. *International journal of molecular sciences*, *22*(16), p.8661.

[3]. Qiblawey, Y., Tahir, A., Chowdhury, M.E., Khandakar, A., Kiranyaz, S., Rahman, T., Ibtehaz, N., Mahmud, S., Maadeed, S.A., Musharavati, F. and Ayari, M.A., 2021. Detection and severity classification of COVID-19 in CT images using deep learning. *Diagnostics*, *11*(5), p.893.

[4]. Nageswaran, S., Arunkumar, G., Bisht, A.K., Mewada, S., Kumar, J.N.V.R., Jawarneh, M. and Asenso, E., 2022. Lung cancer classification and prediction using machine learning and image processing. *BioMed Research International*, *2022*.

[5]. Ruaro, B., Baratella, E., Confalonieri, P., Wade, B., Marrocchio, C., Geri, P., Busca, A., Pozzan, R., Andrisano, A.G., Cova, M.A. and Confalonieri, M., 2021. High-resolution computed tomography: lights and shadows in improving care for SSc-ILD patients. *Diagnostics*, *11*(11), p.1960.

[6]. Maleki, N., Zeinali, Y. and Niaki, S.T.A., 2021. A k-NN method for lung cancer prognosis with the use of a genetic algorithm for feature selection. *Expert Systems with Applications*, *164*, p.113981.

[7]. Monticciolo, D.L., Malak, S.F., Friedewald, S.M., Eby, P.R., Newell, M.S., Moy, L., Destounis, S., Leung, J.W., Hendrick, R.E. and Smetherman, D., 2021. Breast cancer screening recommendations inclusive of all women at average risk: update from the ACR and Society of Breast Imaging. *Journal of the American College of Radiology*, *18*(9), pp.1280-1288.

[8]. Huber, R.M., Cavic, M., Kerpel-Fronius, A., Viola, L., Field, J., Jiang, L., Kazerooni, E.A., Koegelenberg, C.F., Mohan, A., Dos Santos, R.S. and Ventura, L., 2022. Lung cancer screening considerations during respiratory infection outbreaks, epidemics or pandemics: an international association for the study of lung cancer early detection and screening committee report. *Journal of Thoracic Oncology*, *17*(2), pp.228-238.

[9]. Wiesel, O., Sung, S.W., Katz, A., Leibowitz, R., Bar, J., Kamer, I., Berger, I., Nir-Ziv, I. and Mark Danieli, M., 2023. A Novel Urine Test Biosensor Platform for Early Lung Cancer Detection. *Biosensors*, *13*(6), p.627.

[10]. Bhawal, R., Oberg, A.L., Zhang, S. and Kohli, M., 2020. Challenges and opportunities in clinical applications of blood-based proteomics in cancer. *Cancers*, *12*(9), p.2428.

[11]. Jungblut, L., Etienne, H., Zellweger, C., Matter, A., Patella, M., Frauenfelder, T. and Opitz, I., 2023. Swiss Pilot Low-Dose CT Lung Cancer Screening Study: First Baseline Screening Results. *Journal of Clinical Medicine*, *12*(18), p.5771.

[12]. Mellal, M.A. and Zio, E., 2020. System reliability-redundancy optimization with cold-standby strategy by an enhanced nest cuckoo optimization algorithm. *Reliability Engineering & System Safety*, *201*, p.106973.

[13]. Desai, M. and Shah, M., 2021. An anatomization on breast cancer detection and diagnosis employing multi-layer perceptron neural network (MLP) and Convolutional neural network (CNN). *Clinical eHealth*, *4*, pp.1-11.

[14]. Wang, Y., Wu, H., Zhang, J., Gao, Z., Wang, J., Philip, S.Y. and Long, M., 2022. Predrnn: A recurrent neural network for spatiotemporal predictive learning. *IEEE Transactions on Pattern Analysis and Machine Intelligence*, *45*(2), pp.2208-2225.

[15]. Walczak, S., 2019. Artificial neural networks. In *Advanced methodologies and technologies in artificial intelligence, computer simulation, and human-computer interaction* (pp. 40-53). IGI global.

[16]. Shakeel, P.M., Burhanuddin, M.A. and Desa, M.I., 2022. Automatic lung cancer detection from CT image using improved deep neural network and ensemble classifier. *Neural Computing and Applications*, pp.1-14.

[17]. Shakeel, P.M., Burhanuddin, M.A. and Desa, M.I., 2019. Lung cancer detection from CT image using improved profuse clustering and deep learning instantaneously trained neural networks. *Measurement*, *145*, pp.702-712.

[18]. Toğaçar, M., Ergen, B. and Cömert, Z., 2020. Detection of lung cancer on chest CT images using minimum redundancy maximum relevance feature selection method with convolutional neural networks. *Biocybernetics and Biomedical Engineering*, *40*(1), pp.23-39.

[19]. Xie, Y., Meng, W.Y., Li, R.Z., Wang, Y.W., Qian, X., Chan, C., Yu, Z.F., Fan, X.X., Pan, H.D., Xie, C. and Wu, Q.B., 2021. Early lung cancer diagnostic biomarker discovery by machine learning methods. *Translational oncology*, *14*(1), p.100907.

[20]. Ibrahim, D.M., Elshennawy, N.M. and Sarhan, A.M., 2021. Deep-chest: Multi-classification deep learning model for diagnosing COVID-19, pneumonia, and lung cancer chest diseases. *Computers in biology and medicine*, *132*, p.104348.

[21]. Binson, V.A., Subramoniam, M. and Mathew, L., 2021. Detection of COPD and Lung Cancer with electronic nose using ensemble learning methods. *Clinica Chimica Acta*, *523*, pp.231-238.

[22]. Alzubaidi, M.A., Otoom, M. and Jaradat, H., 2021. Comprehensive and comparative global and local feature extraction framework for lung cancer detection using ct scan images. *IEEE Access*, *9*, pp.158140-158154.

[23]. Hatuwal, B.K. and Thapa, H.C., 2020. Lung cancer detection using convolutional neural network on histopathological images. *Int. J. Comput. Trends Technol*, *68*(10), pp.21-24.

[24]. Causey, J.L., Li, K., Chen, X., Dong, W., Walker, K., Qualls, J.A., Stubblefield, J., Moore, J.H., Guan, Y. and Huang, X., 2020. Spatial pyramid pooling with 3D convolution improves lung cancer detection. *IEEE/ACM transactions on computational biology and bioinformatics*, *19*(2), pp.1165-1172.

[25]. Liu, Z., Yao, C., Yu, H. and Wu, T., 2019. Deep reinforcement learning with its application for lung cancer detection in medical Internet of Things. *Future Generation Computer Systems*, *97*, pp.1-9.
[26]. https://www.kaggle.com/code/arnavkj95/candidate-generation-and-luna16-preprocessing

Access this Article in Online	
Quick Response Code	Website: www.ijarm.com Subject: Biomedical Engineering
DOI:10.22192/ijamr.2026.13.04.008	

How to cite this article:
N. Venkatesan, V. Seetha Devi, S. Palani Kumar, D. Balasubramanian. (2026). Lung cancer detection using Wasserstein self-attention Gan and Convorecurart Neural Network (CRANN). Int. J. Adv. Multidiscip. Res. 13(4): 74-98.
DOI: http://dx.doi.org/10.22192/ijamr.2026.13.04.008